Numerical Techniques for Computing Rotordynamic Properties of Mechanical Gas Face Seals

Brad A. Miller
Department of Mechanical and Aerospace Engineering and Engineering Mechanics,
University of Missouri-Rolla,
1870 Miner Circle,
Rolla, MO 65409-0050

Itzhak Green
George W. Woodruff School of Mechanical Engineering,
Georgia Institute of Technology,
Atlanta, GA 30332-0405

The gas film stiffness and damping properties for a spiral grooved mechanical face seal in a flexibly mounted stator configuration are computed using the step jump method and a novel direct numerical frequency response method. The seal model has three degrees of freedom, including axial displacement of the stator and two stator tilts about mutually perpendicular diametral axes. Results from both methods agree well with previously published results computed using the perturbation method, but the two new methods have the advantage of employing computer programs used in the direct numerical simulation of motion. Based on the linearized analysis, the two angular modes are proven to be coupled together and decoupled from the axial mode. Anomalies in the gas film properties tend to occur at large compressibility numbers. The step jump method requires less computing time than the direct frequency response method but at a sacrifice in accuracy at high excitation frequencies. [DOI: 10.1115/1.1467635]

1 Introduction

A schematic for a mechanical face seal is shown (not to scale) in Fig. 1. The face seal is designed to obstruct or prevent gas from escaping from one region to another through a gap between the stator and rotor mating faces. In general, the sealing performance depends greatly on the gap geometry. A smaller gap between the faces allows less leakage and yields a better seal, but zero gap (i.e., face contact) is detrimental because either the faces wear severely or catastrophic seizure occurs. Also, for the same average clearance, seals with more aligned faces generally allow less leakage. To accommodate these criteria, one of the seal elements is flexibly mounted so that its motion will track any misalignments in the rigidly mounted element. A common seal configuration, which is shown in Fig. 1, is one where the stator is flexibly mounted to the housing with a spring or metal bellows and O-ring.

Mechanical face seals are designed to benefit from the relative rotation between the faces allowed by the flexibility in the stator mounting. Relative rotation between the faces results in self-actuating hydrodynamic pressure, which creates a stiff barrier between the seal faces that actively deters face contact. Furthermore, the gas film dissipates energy by internal friction and viscous shearing, which helps to reduce vibrations that result from external disturbances. When designed properly, the gas film dynamic stiffness and damping properties can be beneficial, but they can also be detrimental if the seal is designed improperly. An example of an improperly designed seal is one where the gas film stiffness and damping contribute to a natural resonance close to an operating frequency. It is also imperative to avoid a situation where the gas film damping is negative, which could lead to seal instability. Clearly, the stiffness and damping properties of the gas film are critically important to the successful function and performance of the face seal.

The only technique adopted in the literature for characterizing gas film stiffness and damping properties in spiral grooved face seals or thrust bearings is the small perturbation method. Malanoski and Pan [1] use the technique to study the static and dynamic properties of spiral grooved thrust bearings in axial motion only. Their analysis employs the narrow groove theory (NGT), which assumes that an infinite number of grooves is present and that the gas exhibits quasi-incompressible behavior so that the circumferential fine-scale pressure profile across a period of the groove pattern has a linear zigzag shape. Zirkelback and San Andrès [2] use the small perturbation technique without the NGT restrictions to develop equations that are viable for a seal geometry with a finite number of grooves. These equations are then solved directly using numerical techniques to determine the frequency dependent stiffness and damping coefficients of spiral grooved gas face seals in axial motion only. This technique is also used by Zirkelback [3] to perform a parametric study of these coefficients.

In this work, the gas film stiffness and damping properties will be determined using two new methods. The first is based on the step jump method [4], which characterizes the gas film properties by step responses. The second computes the gas film frequency response using direct numerical time simulation of the pressure field for harmonic motion of the stator. These two techniques have been analytically verified for annular gas squeeze film dampers by Miller and Green [5]. However, mechanical face seals are more complex than squeeze film dampers since cross-coupling effects between the tilt modes are present. It is important to note that no literature has been found that presents the stiffness and damping coefficients for the two tilting modes of the face seal or the coefficients that represent the cross-coupling between the two tilt modes. These tilting modes and the cross-coupling are significant because they play an important role in ''half frequency whirl'' instability that is common in these seals [6].

One advantage of these two techniques is that they employ computer programs similar to the program for the direct numerical time simulation of motion. Therefore, once a computer code has been written to determine the gas film properties, then minimal coding effort is required to simulate the seal motion. On the other hand, the perturbation method would require more time initially in code generation. Even though the perturbation method produces linear equations in the perturbation variables, the solution of these equations requires a fundamentally different procedure than that used by the numerical motion simulation code.

Contributed by the Tribology Division for publication in the ASME JOURNAL OF TRIBOLOGY. Manuscript received by the Tribology Division July 20, 2001; revised manuscript received December 27, 2001. Associate Editor: S. Wu.

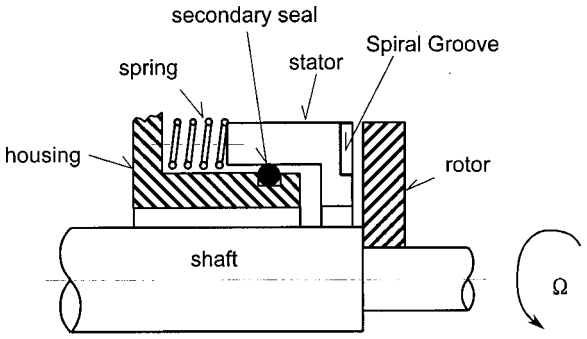

Fig. 1 Schematic of a noncontacting mechanical gas face seal

2 Seal Kinematical Model

A kinematic model of the mechanical seal is shown in Fig. 2. The inertial frame *XYZ* is fixed in space and oriented so the *X* and *Y* axes are in the plane of the rotor and the *Z* axis coincides with the direction of shaft rotation. The stator is flexibly mounted to the housing and has three degrees of freedom. Its position is uniquely defined by tilts (γ_X and γ_Y) about the *X* and *Y* axes, respectively, and the axial translation (*Z*) of the stator center measured from its equilibrium position, C_0. There are N_g spiral grooves at a depth of δ_g on the stator face. The land width to groove width ratio, measured by β, and the equation for the groove curvature are defined as

$$\beta = \frac{w_g}{w_g + w_l}; \quad r = r_i e^{\theta \tan \alpha}, \quad 0 < \alpha < 180 \text{ deg},$$

where α is the spiral angle and $\alpha = 90$ deg corresponds to radial grooves. The radius, r_j, marks the junction between the spiral groove region and the sealing dam region. Spiral grooves are generally oriented so that the natural pumping action opposes the hydrostatic flow of gas, which significantly enhances sealing performance by increasing the load bearing capacity, increasing the gas film stiffness, and reducing leakage.

The applied forces and moments affecting the stator motion come from the support and the gas film pressure. Specifically, the generalized force components from the gas film include the axial force, F_Z, and the respective moments about the *X* and *Y* axes, M_X and M_Y. They are computed by appropriately integrating the pressure over the seal face area. The gas film pressure is a function of the film thickness (h) and its time rate of change ($\partial h/\partial t$), and the relationship among these variables is given by the compressible Reynolds equation [7],

$$\vec{\nabla} \cdot \{ph^3 \vec{\nabla} p - 6\mu \Omega r p h \vec{e}_\theta\} = 12\mu \frac{\partial (ph)}{\partial t}. \tag{1}$$

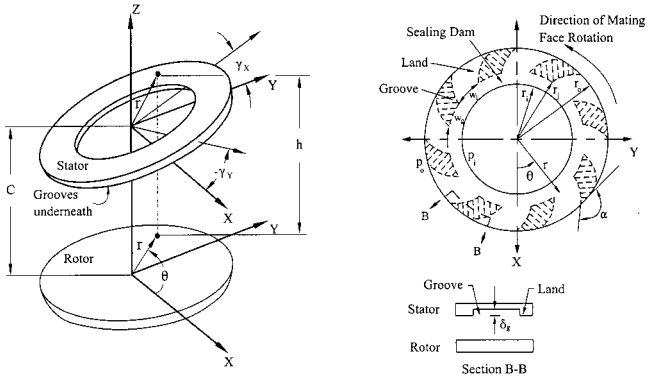

Fig. 2 Mechanical face seal kinematic model

The polar coordinate gradient operator is presumed here because of the geometry, and gas rarefaction effects are ignored. The boundary conditions are

$$p(r_i, \theta, t) = p_i$$

$$p(r_o, \theta, t) = p_o$$

$$p(r, 0, t) = p(r, 2\pi, t).$$

The film thickness and its time derivative are functions of the stator degrees of freedom and their time derivatives,

$$h(r,\theta) = C_0 + Z + r\gamma_X \sin(\theta) - r\gamma_Y \cos(\theta) + \langle \delta_g \rangle$$

$$\frac{\partial h(r,\theta)}{\partial t} = \dot{Z} + r\dot{\gamma}_X \sin(\theta) - r\dot{\gamma}_Y \cos(\theta). \tag{2}$$

Here, the $\langle \delta_g \rangle$ term is only added inside a groove. For simplicity, rotor misalignment is not considered here because it is immaterial when determining the fluid film rotordynamic coefficients.

3 Characterization of Gas Film Stiffness and Damping Properties

The objective of this paper is to characterize the linear reaction of the gas film generalized forces to seal motion. These reactions will be represented by the gas film stiffness (K) and damping (D), which are defined as,

$$K_{i,j} = -\frac{\partial f_i}{\partial x_j}; \quad -D_{i,j} = \frac{\partial f_i}{\partial \dot{x}_j} \quad \begin{matrix} f_1, f_2, f_3 = F_Z, M_X, M_Y \\ x_1, x_2, x_3 = Z, \gamma_X, \gamma_Y \end{matrix}, \tag{3}$$

where f_i and x_j are the generalized gas film force and generalized stator displacement, respectively. For the mechanical seal model shown in Fig. 2, there are a total of nine terms each for the stiffness and damping relating the three generalized forces to each of the three generalized displacements.

Because of compressibility effects, these gas film properties can be viewed in two different ways depending on the type of motion. For small amplitude sinusoidal motion about equilibrium, the gas film exhibits frequency dependent stiffness and damping. The stiffness and damping together make up the complex frequency response,

$$G_{i,j}(\omega) = K_{i,j}(\omega) + j\omega D_{i,j}(\omega), \tag{4}$$

where $j = \sqrt{-1}$ and "i,j" denotes the appropriate generalized force and coordinate. The real part of the frequency response corresponds to the storage modulus, which is the equivalent stiffness that the gas film would exhibit if the stator oscillated at ω in that particular mode. The imaginary part corresponds to the loss modulus, which is equivalent to the product of the damping and the frequency. The loss modulus is a relative measure of the energy dissipation property of the gas film. When the system oscillates at a frequency where the loss modulus is positive (negative), it implies that energy will be removed from (added to) the system. The direct loss modulus has significant implications on stability and performance since it helps to maintain stability if it is positive or forces a system into unstable behavior if it is negative.

A second viewpoint of gas film stiffness is rendered by considering the gas film step response. After a step disturbance in film thickness, gas films exhibit relaxation characteristics similar to viscoelastic materials [8]. This relaxation behavior is captured by the step response ($k(t)$) as defined in Eq. (5),

$$k_{i,j}(t) = -\frac{\delta f_i(t)}{\delta x_j} \quad \begin{matrix} f_1, f_2, f_3 = F_Z, M_X, M_Y \\ x_1, x_2, x_3 = Z, \gamma_X, \gamma_Y \end{matrix}, \tag{5}$$

where $\delta f(t)$ and δx are the deviations of the gas film force and stator position from their equilibrium values. From this definition, it is clear that the step response physically represents the transient gas film stiffness. Again, nine step responses are needed to completely characterize the gas film properties for the face seal. For

linear, time invariant systems, the complex frequency responses can be computed from the step responses using the following integral transformation:

$$G_{i,j}(\omega) \equiv k_{i,j}(0) + \int_0^\infty \dot{k}_{i,j}(\tau) e^{-j\omega\tau} d\tau. \tag{6}$$

The stiffness and damping properties are functions of the characteristic compressibility number (Λ) and the seal geometry, and consequently, they vary with respect to the equilibrium position. In this work, these properties will be calculated with respect to the equilibrium state when the seal faces are perfectly aligned. This equilibrium state provides a standard reference condition regardless of the presence of rotor or stator misalignments, and it is the ''ideal'' design goal where no misalignments from manufacturing or assembly errors are present. Even when misalignments do exist, however, a properly designed seal will maintain small motion about this equilibrium state, so the error introduced in the approximations of the gas film properties would be small as well.

The step jump method and the direct numerical frequency response method are now presented as techniques for computing the linearized gas film properties.

3.1 Step Jump Method. The step response ($k(t)$) has been defined mathematically above in Eq. (5). Numerically calculating the step response begins by computing the steady-state pressure profile at the equilibrium condition of perfect face alignment. Next, a finite step jump away from equilibrium is imposed in a single degree of freedom, which is represented by the generalized coordinate, Δx. After the step jump, the film thickness changes according to Eq. (2). The instantaneous step jump action is assumed to be an isothermal process so that the identity, $ph = \text{constant}$, is valid in the lubrication domain (except at the boundaries) [4,8]. This identity, along with the exception at the boundary, leads to an approximation for the pressure profile immediately after the step jump. Once the pressure after the step has been established, the transient pressure distribution is computed by numerically solving Eq. (1) subject to the boundary conditions, allowing the pressure to diffuse to a new steady-state condition. The step jump formulation is general and can be used with any numerical scheme. However, because the spiral grooved geometry yields a complex film shape in this application, the numerical solution is rendered by a finite element procedure similar to the one in Miller and Green [9]. During the diffusion process, the force and moments are calculated at each instant along with the corresponding time dependent finite step responses as defined by Eq. (7),

$$k_{i,j}(t) \approx -\frac{f_i(t) - f_{eq,i}}{\Delta x_j} \quad \begin{matrix} f_1, f_2, f_3 = F_Z, M_X, M_Y \\ x_1, x_2, x_3 = Z, \gamma_X, \gamma_Y \end{matrix}, \tag{7}$$

where $f_{eq,i}$ is the generalized gas film force at equilibrium. The step amplitudes are chosen to be small ($\Delta Z/C_0 = 0.05$ and $\Delta\gamma_X \cdot r_o/C_0 = 0.04$) with respect to the corresponding equilibrium values.

Equation (7) gives a low order approximation of the step response with an error on the order of $O(\Delta x)$. A higher order approximation is found by averaging the low order responses for steps of Δx, $\Delta x/2$, $-\Delta x/2$, and $-\Delta x$ using

$$k(t) = \frac{1}{6}\{4[k_{\Delta x/2}(t) + k_{-\Delta x/2}(t)] - [k_{\Delta x}(t) + k_{-\Delta x}(t)]\}, \tag{8}$$

where the subscript here denotes the size and direction of the step jump. The error in this approximation is of the order $O(\Delta x^4)$. The ''i,j'' indices are omitted here for clarity, but the same process is used for all the step responses.

Although the face seal model has three degrees of freedom so that nine step responses are theoretically required to characterize the gas film properties, some conditions exist that reduce the number of step response computations needed. First, the moment responses to axial displacements are identically zero, so $k_{M_X,Z}(t) = k_{M_Y,Z}(t) = 0$. Also, natural symmetry conditions yield the following identities: $k_{M_X,\gamma_Y}(t) = k_{M_X,\gamma_X}(t)$ and $k_{M_X,\gamma_Y}(t) = -k_{M_Y,\gamma_X}(t)$. Moreover, the axial force response to a sudden change in tilt is insensitive to the tilt direction if the stator and rotor faces are initially aligned and if the tilt axis is a diameter of the stator. The tilts γ_X and γ_Y satisfy these criterion; therefore, the locus of points relating the axial force and either stator tilt has an inflection point at the equilibrium state. Consequently, the slope at this inflection point (i.e., the stiffness) is zero for all times after the step, i.e., $k_{F_Z,\gamma_X}(t) = k_{F_Z,\gamma_Y}(t) = 0$. The remaining step responses are typically nonzero for the mechanical face seal. As a result of these identities, only step jumps in ΔZ and $\Delta\gamma_X$ are required to characterize all the linearized gas film properties.

Arranging the nonzero stiffness terms into matrix format, as in Eq. (9), it is clear that the axial mode is decoupled from both the tilt modes based on this linearized estimation of the gas film properties,

$$\underline{k}(t) = \begin{bmatrix} k_{F_Z,Z}(t) & 0 & 0 \\ 0 & k_{M_X,\gamma_X}(t) & k_{M_X,\gamma_Y}(t) \\ 0 & k_{M_Y,\gamma_X}(t) & k_{M_Y,\gamma_Y}(t) \end{bmatrix}. \tag{9}$$

Furthermore, the presence of non-zero cross-coupled tilt stiffness terms indicates that the tilt degrees of freedom are coupled.

Once the step responses are computed, the corresponding gas film frequency responses are found by numerically computing the integral in Eq. (6). After this process, a complex frequency response matrix is generated that is populated exactly like the stiffness matrix in Eq. (9).

The step jump method has just one disadvantage. Using the identity, $ph = \text{constant}$, to derive the pressure profile after the step jump leads to a physical impossibility because a pressure discontinuity results at the boundary. This error at low times near $t = 0$ manifests itself as a small error in the high frequency components of the step responses and the corresponding frequency responses. This error will be discussed later in more detail.

3.2 Direct Numerical Frequency Response Method. In the direct numerical frequency response method, the stator is given prescribed harmonic motion at a frequency, ω, so that the film thickness and its time derivative have the form of either

$$\begin{aligned} h(r,\theta) &= h_{eq}(r,\theta) + \Delta Z \cdot \sin(\omega t) \\ \dot{h}(r,\theta) &= \omega \Delta Z \cdot \cos(\omega t), \end{aligned} \tag{10}$$

for computing the gas film reaction to perturbations in Z or

$$\begin{aligned} h(r,\theta) &= h_{eq}(r,\theta) + \Delta\gamma_X\, r \sin(\theta) \cdot \sin(\omega t) \\ \dot{h}(r,\theta) &= \omega \Delta\gamma_X\, r \sin(\theta) \cdot \cos(\omega t), \end{aligned} \tag{11}$$

for computing the gas film reaction to perturbations in γ_X. As with the step responses, symmetry conditions (namely, $K_{M_X,\gamma_X} = K_{M_Y,\gamma_Y}$, $D_{M_X,\gamma_X} = D_{M_Y,\gamma_Y}$, $K_{M_Y,\gamma_X} = -K_{M_X,\gamma_Y}$, and $D_{M_Y,\gamma_X} = -D_{M_X,\gamma_Y}$) render it unnecessary to consider oscillations about the Y axis. The axial displacement and tilt amplitudes are chosen to be small ($\Delta Z/C_0 = 0.05$ and $\Delta\gamma_X \cdot r_o/C_0 = 0.04$) to be within the range of small perturbation theory. Note that $\sin(\omega t)$ does not introduce a step discontinuity in h at $t = 0$.

To compute the frequency responses, either Eq. (10) or Eq. (11), depending on which case is considered, is substituted into Eq. (1). The transient pressure solution is then found by direct numerical solution of the full nonlinear Reynolds equation using a solution procedure similar to the one presented by Miller and Green [9]. Again, the finite element method is conveniently used here because of the groove discontinuity, but when circumstances allow, other numerical schemes can be used as well. The time solution is computed for at least four cycles to ensure that any transient effects have dissipated. Next, the time history of the gas

Table 1 Mechanical face seal parameters

Seal Type	Type I	Type II
Outer Radius, r_o	60.0 mm	60.0 mm
Dam Radius, r_j	51.6 mm	33.72 mm
Inner Radius, r_i	48.0 mm	24.0 mm
Stead-State Clearance, C_0	6.0 μm	6.0 μm
Shaft Angular Velocity, Ω	*see Figs. 3 - 6*	*see Figs. 7 and 8*
Gas Viscosity, μ	$1.8\ (10)^{-5}$ N·s/m^2	$1.8\ (10)^{-5}$ N·s/m^2
Pressure at Inner Radius, p_i	0.2 MPa	0.1 MPa
Pressure at Outer Radius, p_o	0.1 MPa	0.1 MPa
Number of Grooves, N_g	12	50
Spiral Groove Angle, α	160 deg	162.5 deg
Land to Groove Width Ratio, β	0.5	0.6587
Groove Depth, δ_g (μm)	12.0 μm	18.3 μm

film axial force and moments are stored, and the spectra of these results are calculated digitally by a Fourier transform. Then, the gas film frequency responses are found at each excitation frequency using the relations below,

$$G_{i,j}(\omega) = -\frac{f_t(\omega) - f_{eq,i}}{\Delta x(\omega)_j} \quad \begin{matrix} f_1, f_2, f_3 = F_Z, M_X, M_Y \\ x_1, x_2, x_3 = Z, \gamma_X, \gamma_Y \end{matrix} \quad (12)$$

The process above is repeated for multiple oscillation frequencies, sweeping the frequency range of interest to approximate a continuous curve for the frequency response.

3.3 Gas Film Properties. Representative results for the gas film step responses and frequency responses are presented for two mechanical face seals (Type I and II) as a function of shaft speed. The shaft speeds are indicated in the figures, and the other operating conditions and geometrical properties are detailed in Table 1. See nomenclature for normalization of k^* and G^*.

The direct axial step responses, $k_{F_Z,Z}(t)$, for the Type I seal are plotted in Fig. 3. In this figure, the relaxation nature of the gas film is clear. After the step in axial displacement occurs, a pressure differential is created that acts as a restoring force on the stator. The restoring force initially starts at a high value and then decays (or relaxes) to a lower steady-state value. This particular relaxation behavior of gases marks the distinction between compressible and incompressible fluids. The direct tilt step responses, $k_{M_X,\gamma_X}(t)$ and $k_{M_Y,\gamma_Y}(t)$, shown in Fig. 4(*a*) have the same general character as the direct axial step responses; however, for the same Type I seal, the cross-coupled tilt step responses, $k_{M_X,\gamma_Y}(t)$ and $k_{M_Y,\gamma_X}(t)$, are characteristically different (see Fig. 4(*b*)). These step responses start at zero because the initial pressure profiles immediately after the step are symmetric about a diameter perpendicular to the tilt axis. Over time, the shape of the pressure profile rotates in response to the new film thickness forcing the cross-coupled moment to increase, after which the step response eventually levels off to an asymptotic value.

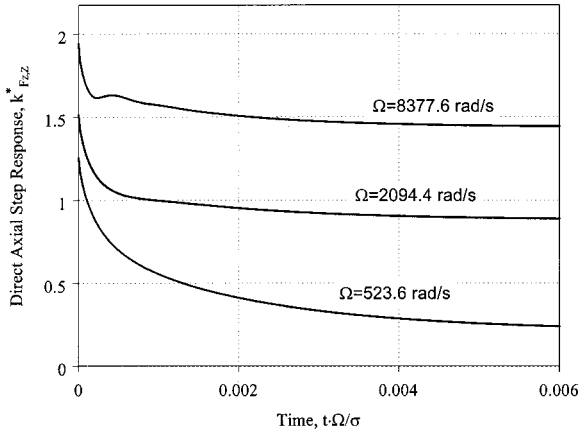

Fig. 3 Direct axial step responses, $k_{F_Z,Z}(t)$, for Seal Type I

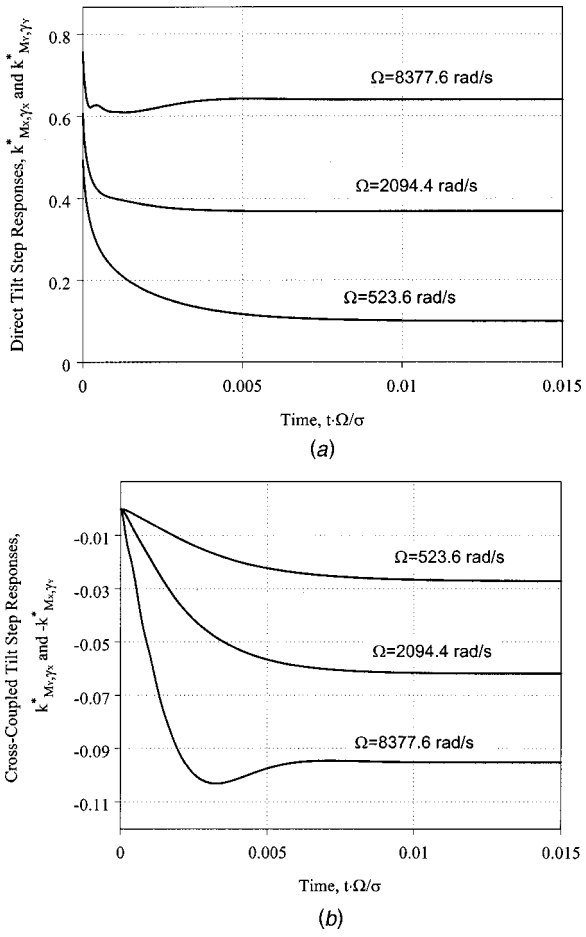

Fig. 4 (*a*) Direct tilt step responses, $k_{M_X,\gamma_X}(t)$ and $k_{M_Y,\gamma_Y}(t)$, for Seal Type I; and (*b*) cross-coupled tilt step responses, $k_{M_Y,\gamma_X}(t)$ and $-k_{M_X,\gamma_Y}(t)$, for Seal Type I

In general, as the shaft speed (and compressibility number, Λ) increases, the amplitudes of the direct step responses tend to increase. However, no general correlation can be drawn between the amplitude of the cross-coupled tilt step responses and the shaft speed.

For large shaft speeds, an anomaly is visible in the shape of the step response curves. Instead of decaying monotonically, a small hump forms in the step response curve (see Figs. 3, 4(*a*) and 4(*b*)). The amplitude of the anomaly tends to increase as the shaft speed (i.e., Λ) increases. This anomaly is also visible in the gas film frequency response, which will be discussed later in more detail.

The frequency dependent nature of the gas film stiffness and damping is evident in the frequency responses plotted in Figs. 5–8. These figures qualitatively display the agreement between the direct numerical frequency response method and the step jump method. Note in Figs. 5 and 6(*a*) that the step jump method tends to underestimate the direct frequency responses at high frequencies. This relatively small error at high frequencies is inherent in the step jump method, resulting from the assumed non-physical gas pressure discontinuity at the boundaries at $t=0$. For the direct

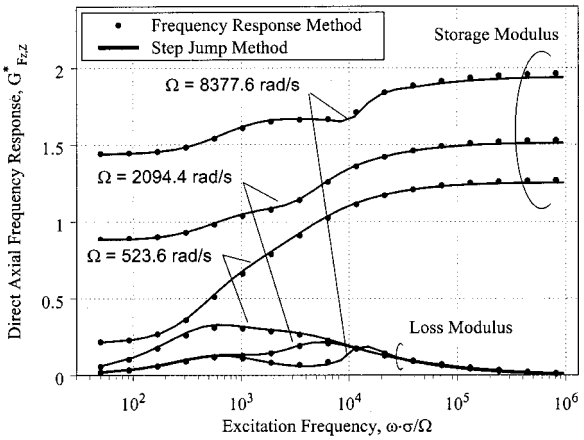

Fig. 5 Direct axial frequency responses, $G_{F_{Z},Z}$, for Seal Type I

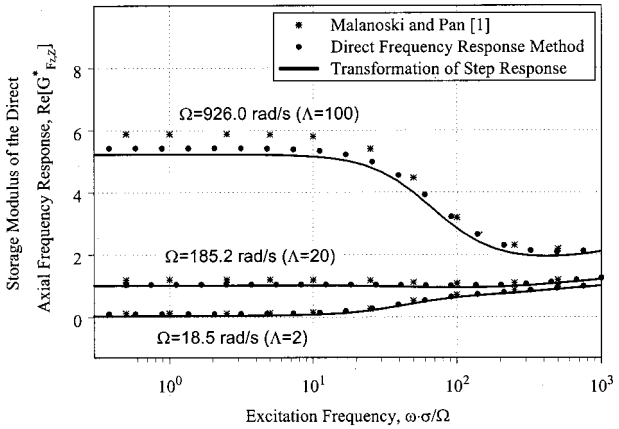

Fig. 7 Comparison of storage Moduli for the direct axial frequency responses, $G_{F_{Z},Z}$, for Seal Type II

axial frequency response shown in Fig. 5, the gas film stiffness (storage modulus) generally tends to increase with increasing shaft speed. Also, at frequencies above approximately $\omega \cdot \sigma/\Omega = 2(10)^4$, the loss properties are constant regardless of the shaft speed. The direct tilt frequency responses shown in Fig. 6(*a*) are similar in nature to the direct axial frequency response. However, the cross-coupled tilt frequency responses shown in Fig. 6(*b*) are quite different in character than the direct frequency responses. Because the pressure profile rotates about the Z axis with rotor rotation, the storage modulus for G_{M_Y,γ_X} and the loss modulus for G_{M_X,γ_Y} are negative.

The anomaly evident in the gas film step responses for seals with large compressibility numbers is also visible in the direct frequency responses (see Figs. 5 and 6(*a*)). An explanation of this phenomenon can be found from a dimensional analysis of the Reynolds equation [10]. As the spacing decreases and the shaft speed increases (i.e., Λ gets larger), the term $ph^3\nabla p$ in the Reynolds equation, Eq. (1), becomes progressively insignificant and tends toward zero. In the steady-state case, this leads to a limiting solution of $ph=$ constant [7]. However, for the transient case, the unsteady term remains and the Reynolds equation simplifies to

$$F\{ph\}=0, \tag{13}$$

where F is an operator of the form

$$F=\Omega\frac{\partial}{\partial\theta}+2\frac{\partial}{\partial t}. \tag{14}$$

Consider first a dimensional analysis for a flat faced (ungrooved) seal. In this case, logical characteristic values for θ and t are the full circumferential angle, 2π, and the reciprocal of the excitation frequency, $1/\omega$, respectively. In this case, the following substitutions can be made: $\partial/\partial\theta \rightarrow 1/(2\pi)$ and $\partial/\partial t \rightarrow -\omega/(2\pi)$. Here, the F operator becomes zero when $\omega=\Omega/2$, which corresponds to

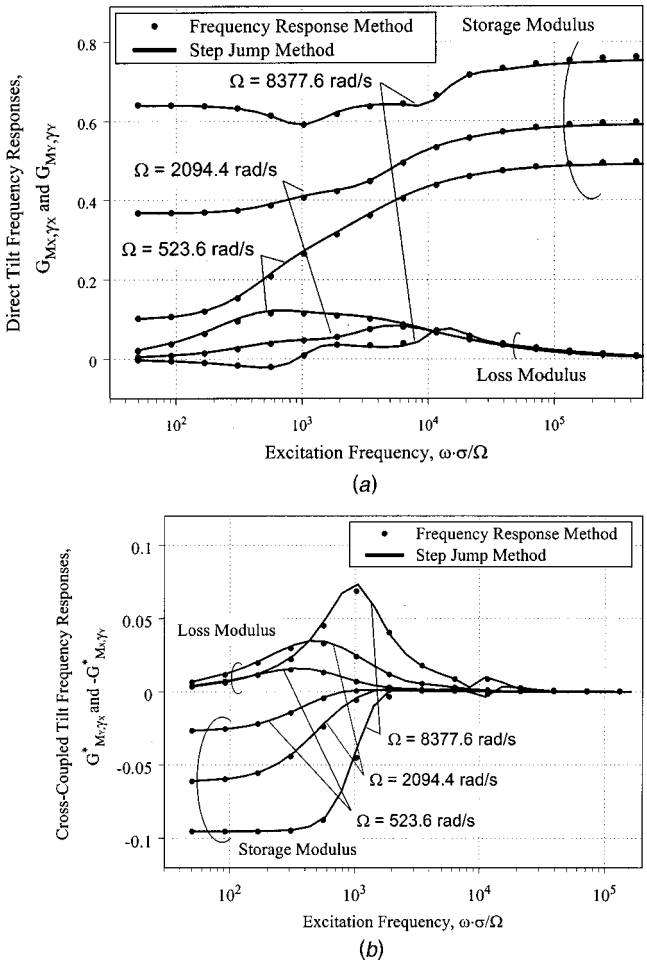

Fig. 6 (*a*) Direct tilt frequency responses, G_{M_X,γ_X} and G_{M_Y,γ_Y}, for Seal Type I; and (*b*) cross-coupled tilt frequency responses, G_{M_Y,γ_X} and $-G_{M_X,\gamma_Y}$, for Seal Type I

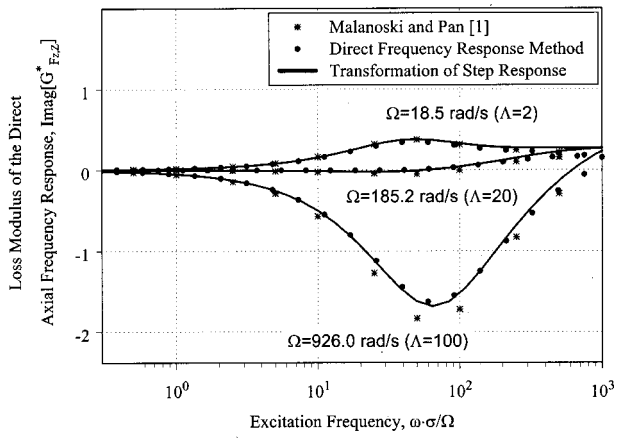

Fig. 8 Comparison of loss Moduli for the direct axial frequency responses, $G_{F_{Z},Z}$, for Seal Type II

gas film instabilities at half the shaft speed. Therefore, according to this dimensional analysis, gas film instabilities develop a "half frequency whirl" at operating conditions when the compressibility number is large.

The dimensional analysis above is specifically valid for flat faced seals, in which case the anomalies manifest as sharp peaks in the frequency responses at exactly half the shaft speed as the dimensional analysis predicts. However, in this case with spiral grooves, the anomalies manifest as small humps with a larger frequency content not necessarily limited to a small range close to half the shaft speed. The discrepancy results because the previous dimensional analysis does not account for the pattern of film thickness discontinuities at the boundaries of the spiral grooves. These discontinuities disrupt the flow and alter the characteristic values, which tend to increase the average frequency content of the anomaly and smear it over a larger frequency range.

Recall previously that the coupled axial-force/tilt step responses ($k_{F_Z,\gamma_X}(t)$ and $k_{F_Z,\gamma_Y}(t)$) were zero; consequently, the corresponding frequency responses (G_{F_Z,γ_X} and G_{F_Z,γ_Y}) computed from these step responses are also identically zero. However, when computed by the direct frequency response method, these cross-coupled frequency responses are not zero. The direct numerical frequency response method computes the gas film frequency response at discrete frequencies over the frequency range of interest. For example, when the cross-coupled coefficient $G_{FZ,\gamma X}$ is computed at a one single frequency, the stator tilt γ_X is driven at a prescribed singular harmonic oscillation and the gas film response is computed by a full numerical solution of the unsteady, nonlinear Reynolds equation. Even though the film thickness profile is anti-symmetric with respect to the X axis at all times during this process, the nonlinear pressure solution does not yield a corresponding anti-symmetric pressure field. Therefore, a nonzero value for the net axial force response at the driving frequency results because of the nonlinearities in the Reynolds equation. Although the cross-coupled axial force responses G_{F_Z,γ_X} and G_{F_Z,γ_Y} are present in this case, their amplitudes are relatively small compared to the direct moment responses and the direct axial response, so they can be neglected. This result confirms the conclusion that, based on a linearized gas film analysis, the two tilt modes are coupled to each other and decoupled from the axial mode.

For validation purposes, results from the two new methods detailed here are compared to previously published data in Figs. 7 and 8. The geometry and operating conditions for comparison are indicated in Table 1 as Seal II. Note that Seal II is effectively a thrust bearing since no pressure differential exists. This particular bearing has been analyzed previously using the Narrow Groove Theory by Malanoski and Pan [1], who give only the direct axial force response, $G_{F_Z,Z}$. The results from all three methods are in qualitative agreement, and the differences can be attributed to the assumptions made in the Narrow Groove Theory. Zierkelback and San Andrès [2] also present results for this case from a small perturbation analysis without the Narrow Groove Theory assumptions, and their results match the results given here very well.

It is important to note that no data has been found in the literature regarding the properties of the tilt modes for mechanical gas face seals. They are given here for the first time.

4 Numerical Considerations

Table 2 gives a brief comparison of the relative CPU times needed to compute the results from the step jump method and the direct numerical frequency response method. The values represent the times needed to compute all the responses required to fully characterize the gas film properties, including the time needed to compute the steady-state pressure profile. These numerical solutions were computed with a code employing the finite element method solution procedure described in Miller and Green [9]. However, in [9], the equations of motion are solved, but they are irrelevant here. Therefore, that solution is bypassed. Also, since tilt modes are included by this analysis, axisymmetric or antisymmetric conditions do not exist so the pressure solution must be computed over the full seal circumference, which requires many more nodes than the axisymmetric case. According to Table 2, the step jump method is approximately two to three times faster than the direct numerical frequency response method. However, a tradeoff exists because the step responses inherently contain a small error at high frequencies. Choosing the best method for a given application requires balancing the computing time and the degree of accuracy desired.

Table 2 Comparison of relative CPU times for the step jump method and the direct numerical frequency response method

Shaft Speed (rad/s)	Step Response Relative CPU Time*		Direct Numerical Frequency Response Relative CPU Time*	
	$k_{FZ,Z}$ (Fig. 3)	$k_{MX,\gamma X}$, $k_{MY,\gamma Y}$, $k_{MY,\gamma X}$, and $-k_{MX,\gamma Y}$ (Fig. 4a and 4b)	$G_{FZ,Z}$ (Fig. 5)	$G_{MX,\gamma X}$, $G_{MY,\gamma Y}$, $G_{MY,\gamma X}$, and $-G_{MX,\gamma Y}$ (Fig. 6a and 6b)
Ω=523.6	1.0	1.0	2.6	2.0
Ω=2094.4	1.2	1.2	3.0	2.3
Ω=8377.6	1.2	1.2	3.0	2.3

*Normalized by 485 minutes, the CPU time for $k_{FZ,Z}$@ Ω=523.6 rad/s on a workstation with a PA-RISC 8200 processor at 200 MHz.

5 Conclusions

Two new methods have been developed for characterizing the properties of gas lubricated mechanical face seals. One technique is based on the step jump method, which characterizes the properties in the time domain using the step responses. To get the corresponding frequency responses, a numerical integral transformation is performed on the step responses. The other method is a direct numerical technique based on a full nonlinear numerical simulation of motion. The results from both methods agree well with each other and with published results. However, because of the inherent error in the step response at low times near $t=0$, the step jump method tends to underestimate the frequency responses at large frequencies. On the other hand, the step jump method offers an advantage of being two to three times faster in computation than the direct numerical frequency response method. The time savings may vary depending on the application and how many data points are needed for the direct numerical method. The advantages and disadvantages of each method must be weighed to determine the appropriate technique to use for a given situation.

Based on a linear approximation of the gas film properties, the gas film stiffness and damping matrix for mechanical face seals is semi-diagonal. This diagonalization indicates that the two tilt modes are coupled together and decoupled from the axial mode with regard to the gas film effects. This represents a powerful function of linearized techniques to offer new insights into the dynamic characteristics of gas lubricated triboelements.

Acknowledgment

This work was supported in part by an NSF Graduate Research Traineeship through Grant No. EEC-9256289 while the first author was at the Georgia Institute of Technology. This support is gratefully acknowledged.

Nomenclature

C = clearance between the rotor and stator, C_0+Z
C_0 = design clearance between rotor and stator at equilibrium
$D_{i,j}$ = gas film damping
$\hat{e}_\theta$ = unit vector along θ direction

F = differential operator, $\Omega\partial/\partial\theta+2\partial/\partial t$
F_Z = gas film axial force
f_i = generalized force: F_Z, M_X, or M_Y
δf_i = transient change in a generalized force from the equilibrium value
f_{eq} = generalized force at equilibrium
$G_{i,j}$ = gas film frequency response, $G_{i,j}=K_{i,j}+j\omega D_{i,j}$
$G^*_{i,j}$ = nondimensional frequency response; axial, $G^*=G\cdot C_0/(P_a r_o^2)$; tilt, $G^*=G\cdot C_0/(P_a r_o^4)$
h = film thickness separating stator and rotor
h_{eq} = film thickness at equilibrium
j = imaginary number, $\sqrt{-1}$
$K_{i,j}$ = gas film stiffness
$k_{i,j}$ = gas film step response
$k^*_{i,j}$ = nondimensional step response; axial, $k^*=k\cdot C_0/(P_a r_o^2)$; tilt, $k^*=k\cdot C_0/(P_a r_o^4)$
$\underline{k}$ = step response matrix
M_X, M_Y = gas film moments about X and Y axes
N_g = number of grooves
P_a = ambient pressure
p = gas pressure
p_i, p_o = gas pressure at inner and outer radial boundaries
r = radius, radial coordinate
r_i, r_o, r_j = inner, outer and sealing dam radii
t = time
w_g, w_l = width of groove and land regions
XYZ = inertial reference frame
x_i = generalized coordinate or degree of freedom: Z, γ_X, or γ_Y
δx = infinitesimal change in a generalized coordinate from the equilibrium value
Δx = finite step change in a generalized coordinate from the equilibrium value
Z = axial displacement of stator from equilibrium clearance
ΔZ = amplitude of step jump in Z
α = spiral groove angle
β = groove width ratio, $w_g/(w_g+w_l)$
δ_g = groove depth
γ_X, γ_Y = stator tilt about X and Y axes
$\Delta\gamma_X$ = amplitude of step jump in γ_X
θ = circumferential coordinate
Λ = compressibility number, $6\mu\Omega r_o^2/(P_a C_0^2)$
μ = gas viscosity
σ = squeeze number, $12\mu\Omega r_o^2/(P_a C_0^2)$
Ω = shaft rotational speed
ω = excitation frequency

Subscripts

i = corresponding to the generalized forces: F_Z, M_X, or M_Y
j = corresponding to the generalized coordinates: Z, γ_X, or γ_Y

References

[1] Malanoski, S. B., and Pan, C. H. T., 1965, "The Static and Dynamic Characteristics of the Spiral-Grooved Thrust Bearing," ASME J. Basic Eng., **87**, pp. 547–558.
[2] Zirkelback, N., and San Andrès, L., 1999, "Effect of Frequency Excitation on Force Coefficients of Spiral Groove Gas Seals," ASME J. Tribol., **121**, pp. 853–863.
[3] Zirkelback, N., 2000, "Parametric Study of Spiral Groove Gas Face Seals," J. Tribol. Trans., **43**, pp. 337–343.
[4] Elrod, Jr., H. G., McCabe, J. T., and Chu, T. Y., 1967, "Determination of Gas-Bearing Stability by Response to a Step-Jump," ASME J. Lubr. Technol., **89**, pp. 493–498.
[5] Miller, B., and Green, I., 2000, "The Dynamic Properties of Annular Gas Squeeze Film Dampers," Tribol. Trans., **43**, pp. 302–310.
[6] Green, I., and Etsion, I., 1985, "Stability Threshold and Steady-State Response of Noncontacting Coned-Face Seals," ASLE Trans., **28**, pp. 449–460.
[7] Gross, W. A., 1980, *Fluid Film Lubrication*, John Wiley & Sons, New York.
[8] Miller, B., and Green, I., 1997, "On the Stability of Gas Lubricated Triboelements Using the Step Jump Method," ASME J. Tribol., **119**, pp. 193–199.
[9] Miller, B., and Green, I., 2001, "Numerical Formulation for the Dynamic Analysis of Spiral-Grooved Gas Face Seals," ASME J. Tribol., **123**, pp. 395–403.
[10] Ono, K., 1975, "Dynamic Characteristics of Air-Lubricated Slider Bearing for Noncontact Magnetic Recording," ASME J. Lubr. Technol., **97**, pp. 250–260.